Conserved neural circuit structure across *Drosophila* larval development revealed by comparative connectomics

Stephan Gerhard[*1], Ingrid Andrade[†1], Richard D. Fetter[‡1], Albert Cardona[§1], and Casey M. Schneider-Mizell[¶1]

[1]Janelia Research Campus, Howard Hughes Medical Institute, Ashburn, USA

May 30, 2017

[*]Current address: Friedrich Miescher Institute, Basel, Switzerland
[†]Current address: Department of Molecular, Cell and Developmental Biology, University of California Los Angeles, Los Angeles, USA
[‡]Current address: Department of Biochemistry and Biophysics, University of California, San Fransisco, San Fransisco, USA
[§]Co-corresponding: cardonaa@janelia.hhmi.org
[¶]Co-corresponding: schneidermizellc@janelia.hhmi.org

Abstract

Throughout an animal's postembryonic development, neuronal circuits must maintain appropriate output even as the body grows. The contribution of changes to circuit structure – neuronal morphology and synaptic connectivity – to postembryonic circuit development remains unclear. Here, we used new and existing serial section electron microscopy volumes to reconstruct and compare an identified nociceptive circuit in two *Drosophila* larvae at early and late stages. We found extremely consistent, topographically-arranged circuit structure. Five-fold increases in size of interneurons were associated with compensatory structural changes that maintained cell-type-specific synaptic input as a fraction of total inputs. An increase in number of synaptic contacts was accompanied with a disproportionate increase in the number of small dendritic terminal branches relative to other neuronal compartments. We propose that these precise patterns of structural growth act to conserve the computational function of a circuit, for example determining the location of a nociceptive stimulus.

Introduction and Results

As an animal undergoes postembryonic development, its nervous system must continually adapt to a changing body. While circuit remodeling can generate new behaviors, such as the addition of new swimming strategies in zebrafish [1], in many cases the functional role of a circuit is conserved as an animal grows. Functional conservation through postembryonic development in neuronal morphology or number has been observed throughout sensory-motor processing, from maintenance of spatial receptive fields of mechanosensory neurons in *Drosophila* larva [2], to frequency selectivity in cricket interneurons [3], to motor neuron rhythms in crustacean stomatogastric ganglion [4], and muscle responses at the *Drosophila* larva neuromuscular junction [5–7].

Homeostatic plasticity has been proposed as a key mechanism for the maintenance of circuit output. Neuronal function arises through the combination of morphology, connectivity, and ion channel distributions, and each of these properties can be continually adjusted to keep the functional output of a cell consistent in an uncertain or changing environment [4, 8–11].

The nature and extent of postembryonic circuit development through structural changes — for example by neurons growing in size, adding branches, or adding new synaptic connections as opposed to intrinsic functional changes like ion channel distribution — remains unclear. One hint comes from studies of circuit variability, which reflects differences in the outcome of similar developmental processes. Rhythm-generating networks such as the crustacean stomatogastric ganglion and leech heartbeat network exhibit large inter-animal variations in morphological structure [12] and functional connection strength [13–15], with concomitant adaptation in intrinsic properties [16] nonetheless permitting consistent rhythmic activity patterns [17, 18]. However, studies of sensory systems in *Drosophila* using electron microscopy (EM) have found low intra-animal variation in number of synaptic contacts between neurons in the adult visual system [19] and larval mechanosensatory [20] and olfactory [21] systems, suggesting that different computational properties of circuits might exert more or less selective constraints on their structural development.

Here, we used detailed circuit reconstruction from EM to study the circuitry of identified neurons across postembryonic development in the *Drosophila melanogaster* larva. Between hatching and pupariation, larvae increase in surface area by two orders of magnitude [5] and neurons become larger and have more synapses [22], but almost no new neurons are added [23] and behavior is largely unchanged. We focused on circuitry related to multidendritic class IV sensory neurons (mdIVs), which respond to

noxious or damaging stimulus [24]. For the EM volume of a 1st instar larva (L1v), we used a previously reported EM volume that covers the central nervous system (CNS) of a larva 6 hour post-hatching [20]. For the EM volume of a 3rd instar larva (L3v), we generated a new EM volume of several abdominal segments of a wandering 3rd instar larva, approximately 96 hours post-hatching (Figure 1—figure supplement 1A,B).

We first considered the structure of mdIV terminals at different stages (Figure 1). The mdIV terminals in abdominal segment A1 were previously reconstructed in the L1v [20]. To map terminal morphology in a 3rd instar larva, we used CATMAID [25] to manually reconstructed in the L3v the morphology and synapses of the six mdIV terminals (three per hemisegment) in abdominal segment A3 (Figure 1A and Figure 1—figure supplement 1C), which was chosen because of its centrality in the EM volume and lack of nearby section gaps. Identity of mdIV terminals and their subtypes was determined based on stereotyped morphological features such as antero-posterior projections, midline crossing, and nerve bundle (Figure 1B) [20, 26, 27]. Terminals maintained a similar morphology (Figure 1B and Figure 1—figure supplement 2), while the number of synaptic outputs increased by a factor of 4.7, from a mean of 185 synapses per terminal to 872 synapses per terminal (Figure 1C–D). Insect synapses are polyadic, with multiple postsynaptic targets per presynaptic site [28]. We found no significant difference between the distribution of number of postsynaptic targets for mdIV presynaptic sites in the L1v compared to the L3v (Figure 1E), suggesting the structure of individual polyadic synapses remains unchanged.

To discover and map all neurons monosynaptically connected to mdIVs, we reconstructed neurites starting at every synaptic contact on the mdIV terminals in the L1v (Figure 2A), extending previous work [20]. We found 13 distinct cell types (Figure 2—figure supplement 1). Five types were local neurons (LNs), with dendrites covering one or two segments (Figure 2B); three were regional, with dendrites covering three to five segments; four had processes projecting from posterior to anterior across the entire VNC; and one was a descending neuron with an axon that projected across the whole VNC (Figure 2—figure supplement 1A). One cell type, A02n, was comprised of two indistinguishable cells per hemisegment, unusual for larval neurons. First order nociceptive targets formed a sparse network (Figure 2—figure supplement 2B). We found a feedback motif for presynaptic modulation of mdIV terminals, but no densely connected local interneurons such as those found in *Drosophila* early sensory processing areas for olfaction [21, 29] or mechanosensation [30, 31].

To measure how circuit structure changes through larval growth, we reconstructed the twelve LN cells in segment A3 in the L3v, as those were the only cell types that would be fully contained in the volume (Figure 2C). All LNs were morphologically identifiable, despite increases in size, arbor complexity, and synaptic count (Figure 2B,D). Axons and dendrites differed in their morphological growth. Total dendritic cable length increased by a factor of 4.69 ± 0.28, consistent with the increase measured from light microscopy in larval motor neurons [22], while axonal cable increased by a factor of 2.08 ± 0.22 (Figure 2E–H), similar to the overall 1.7–1.8 times scale-up of neuropile width (from 43 μm to 72 μm) and segment length (from 15 μm to 27 μm). The number of synaptic inputs onto LN dendrites increased by a factor of 5.28 ± 0.52 (Figure 2I,K), while inputs onto axons increase only by 2.34 ± 0.32 (Figure 2—figure supplement 4A). Axonal output by interneurons increased by a factor of 3.36 ± 0.61, slightly less than the factor of 4.7 observed in sensory terminals (Figure 2J,K). All three LN types for which dendritic synaptic outputs were present in the L1v also had dendritic outputs in the L3v (Figure 2—figure supplement 4B,C). Indeed, the segregation index, a measure of the segregation of synaptic inputs and outputs [25], remained similar for each neuron across development (Figure 2—figure supplement 4D).

We next considered synaptic connections between mdIVs and LNs (Figure 1—figure supplement 1D–F). All LNs in L3v maintained input from mdIVs (Figure 2L), receiving on average 5.7 times more synapses than in the L1v (Figure 2N). In spite of the increase in synapse number, the fraction of total dendritic inputs from each mdIV type was significantly correlated between the L1v and L3v (Figure 2O,P), suggesting that the relative input from each mdIV type is conserved, preserving the topographical structure of LN mdIV input (Figure 2—figure supplement 2A–C). Interestingly, the variability in connection weight between mdIV types and left/right homologues of LNs decreased between the L1v and L3v, suggesting a convergence over time of connectivity weight onto a common value (Figure 2Q).

A postsynaptic neuron can only connect to presynaptic sites that are nearby in space. Numerically strong connections could arise either due to a low probability of connecting to many nearby potential synapses, or to a high probability of connecting to fewer potential synapses (Figure 2—figure supplement 3A,B) [32]. We found that in both the L1v and L3v, the fraction of potential synapses that were connected ranged from 0.01–0.47 and correlated strongly with the overall numerical strength of a connection, suggesting that the latter is true (Figure 2—figure supplement 3C,D). Moreover, the probability of connection was well-correlated between the L1v and L3v (Figure 2—figure supplement 3E), suggesting that synaptic specificity in terms of the growth and connectivity of terminal branches was consistent across larval development.

Most terminal branches in *Drosophila* are 'twigs', short microtubule-free processes that receive the majority of synaptic input [25, 33] (Figure 3A,B), in contrast to the contiguous microtubule-containing neuronal "backbone" that spans the soma and main branches. To understand how twigs and backbones change over development, we manually identified all twigs in the LNs (Figure 3—figure supplement 1.) We found that the number of twigs increased by an average factor of 2.70 ± 0.36 (Figure 3C). The total length of cable that twigs span increased by a factor of 5.1 ± 0.24, significantly more than backbone (2.08 ± 0.22) (Figure 3D). While the fraction of dendritic cable comprised of twigs remained similar (Figure 3E,F), the fraction of dendritic input synapses onto twigs increased to 0.86 (Figure 3G,H). Taking into account only the topological structure of neuronal arbors (as measured by Strahler number [34] (Figure 3I,J)), we found that the fraction of dendritic cable that is terminal or next-to-last order is similar not only across development, but across cell types (Figure 3K). Taken together, this suggests that neurons grow by greatly increasing the number of twigs, while more modestly increasing the length of the backbone neurites from which they sprout.

To understand how twigs change over development, we analyzed twigs in the L1v and L3v as distinct arbors. Typical twigs in both the L1v and L3v are short (median twig length — L1v: 0.99 μm; L3v: 1.6 μm), have few branch points (median branch points per twig — L1v: 0; L3v: 0) and few postsynaptic sites (median synapses per twig — L1v: 1; L3v: 2) (Figure 4A–D). However, twigs in the L3v are consistently slightly longer than their L1v counterparts, possibly reflecting the overall increase in neuropil dimensions. The median distance between adjacent twigs along neuronal backbone remains similar (L1v: 0.83 μm; L3v: 1.03 μm), as well. Twig properties and their development are qualitatively similar for each cell type, although in some cases there are modest quantitative differences (Figure 4—figure supplement 1).

Connections between neurons are often comprised of multiple synaptic contacts. We previously found that numerically strong connections are distributed across many twigs in 1st instar motor neuron dendrites [25]. This remains true for connections from mdIV terminals to LN dendrites in both the L1v and L3v, with approximately one twig for every 2.5 synapses in numerically strong connections (Figure 4E). In spite of the increased numerical strength of connections, 81% of twigs host only one or two synapses of a given connection in the L3v (Figure 4F,G).

Numerically strong, anatomically distributed connectivity makes reconstructions robust to random errors or intentionally incomplete sampling of small processes. For each mdIV-to-LN connec-

tion, we simulated removing twigs from our anatomical reconstructions with a given omission/error probability between 0 and 1 (N=5000 simulations per value), and measured the fraction of observed synapses that would remain (Figure 4H,I). For each connection, we measured the maximum error rate for which the probability of detecting fewer than 25% of the observed synapses was was $\leq$5% (Figure 4H,I). Redundancy resulted in connections that would be detectable even if twigs were missed at the same rate (12%) as observed in previous work with the same method (Figure 4I). Numerically strong connections in the L3v, in particular, would still be detectable with a 50% error rate, suggesting that a strategy of incomplete sampling could quickly identify numerically strong synaptic partners at the cost of precise measurement of connectivity weight.

Discussion

Our results demonstrated that a collection of structural features conserved through larval development underly stereotypy in *Drosophila* larval nociceptive circuits. This establishes a quantitative foundation for the qualitative observation that circuit connectivity in the L1v predicted the presence of functional connectivity in 3rd instar larvae [20, 30, 35–37]. The anatomical elements of connectivity, polyadic synapses and small postsynaptic twigs, remain extremely similar. Connection specificity was maintained not only in the identity of synaptic partners, but in the relative weight of connection strength. This acts to preserve key circuit properties, such as topographic receptive fields that could aid in detecting the location of a nociceptive stimulus. Stringent structural stereotypy stands in contrast to rhythm-generating circuits in other invertebrates, in which variability in morphology and functional properties can be large [12–15]. One possibility is that the computation of certain features from sensory input imposes tighter constraints on circuit structure than the production of periodic activity. This is consistent with a recent EM analysis of the adult *Drosophila* that found high variability in dendritic length and number of synapses in olfactory projection neurons, with arbor size and number of synaptic inputs correlated in a manner well-posed to evoke consistent postsynaptic responses [38]. We note that sensory synapses are excitatory, and it will be an interesting avenue of future work to examine if inhibitory connections follow similar developmental rules.

Nonetheless, many features of neurons changed across development. Axons and dendrites grew in length and number of synapses to differing degrees, suggesting that the mechanisms underlying development act differently in different compartments. Interestingly, although cell types varied

considerably in size at any given time point, the fold-increase in total cable length and synapse count was nearly constant across cell types. This suggests that if neurons have overall size [39] or excitability targets [10], these targets increase at an approximately common rate across cell types. We propose that combining observations of precise structural changes described here with cell-type specific genetic reagents in *Drosophila* larva [40, 41] offers a powerful system to elucidate the mechanisms underlying development and homeostatic compensation in neuronal circuits.

Acknowledgements

We would like to thank Stephan Saalfeld for assistance registering the L3v, Maarten Zwart, Mattias Landgraf, Chris Doe, and Marta Zlatic for useful comments, and James Truman for generously sharing light microscopy data to help identify neurons. This work was funded by the Howard Hughes Medical Institute.

Methods

Sample preparation and electron microscopy

The L1v is fully described in [20]. In brief, the central nervous system from a 6 hour old *[iso] Canton S G1 x* w^{1118} *[iso] 5905* female larva were dissected and, after chemical fixation, stained *en bloc* with 1% uranyl acetate. Serial 50 nm sections were cut and stained with uranyl acetate and Sato's lead [42]. Sections were imaged at 3.8×3.8 nm using Leginon [43] on an FEI Spirit TEM (Hillsboro). Images were montaged in TrakEM2 [44, 45] and aligned using elastic registration [46].

For the L3v, the central nervous systems from a wandering 3rd instar *[iso] Canton S G1 x* w^{1118} *[iso] 5905* larva was dissected in PBS and immediately transferred to 125 μl of 2% glutaraldehyde in 0.1 M Na cacodylate buffer, pH 7.4 in a 0.5 dram glass vial (Electron Microscopy Sciences, cat. no. 72630-05) on ice. 125 μl of 2% OsO_4 in 0.1 M Na-cacodylate buffer, pH 7.4 was then added and briefly mixed immediately before microwave assisted fixation on ice conducted with a Pelco BioWave PRO microwave oven (Ted Pella, Inc.) at 350W, 375W and 400W pulses for 30 sec each, separated by 60 second intervals. Samples were rinsed 3 x 30 sec at 350W with 0.1 M Na-cacodylate buffer, separated by 60 sec intervals,

and post-fixed with 1% OsO_4 in 0.1 M Na-cacodylate buffer at 350W, 375W and 400W pulses for 30 sec each, separated by 60 sec pauses. After rinsing with distilled water 3 x 30 sec at 350W with 60 sec pauses between pulses, the samples were stained *en bloc* with 7.5% uranyl acetate in water overnight at 4° C. Samples were then rinsed 3×5 min with distilled water, dehydrated in an ethanol series followed by propylene oxide, infiltrated and finally embedded in Epon resin. Serial 50 nm sections were cut using a Diatome diamond knife and a Leica UC6 ultramicrotome, and picked up on Pioloform support films with 2 nm C on Synaptek slot grids. Sections were stained with uranyl acetate followed by Sato's lead [42] prior to imaging. An FEI Spirit TEM operated at 80kV was used to image the serial sections at 2.3 x 2.3 nm pixel resolution using Leginon [43].

L3v image volume registration

The L3v consisted of ≈300,000 4k×4k image tiles, which were montaged and aligned using linear and nonlinear methods [46] in TrakEM2 [45]. Filters for brightness and contrast correction were applied before montaging (Default min and max, normalized local contrast, enhance contrast). Images were first montaged in a section with two passes of linear montaging, first targeting only a translation transformation (correspondence weight 1.0), and in the second pass targeting an affine transformation. This was followed by an elastic, non-linear montaging pass. For alignment between sections, parameter exploration was performed on a scaled down substack (scale factor 10) of 5 sections, targeting extraction of approximately 2000 features, 100 correspondences and an average displacement of 10 pixels. Linear alignment was applied to all sections using an affine transformation model. The "Test Block Matching Parameters" tool (http://imagej.net/Test_Block_Matching_Parameters) was used on 5 adjacent sections to find optimal parameters for the elastic registration pass. Elastic alignment was applied with local smoothness filter approximating an affine local transformation. The resulting aligned image stack was exported to an image tile pyramid with six scale levels for browsing and circuit reconstruction in CATMAID [25, 47]. The L3v image stack is available at (*https://neurodata.io/*).

Neuron reconstruction

For the annotation of mdIV targets in the L1v, we manually reconstructed all neurons pre- and post-synaptic to the previously-described mdIV terminals in segment A1 [20]. Circuit reconstruction in both datasets was performed in CATMAID following annotation and review procedures described previ-

ously [25]. For 1004/1096 post-synaptic connections and 85/85 pre-synaptic connections, we were able to reconstruct an identifiable neuron. This included 173 neurites spanning a total of 30.2 mm, 13,824 synaptic inputs, and 18,624 synaptic outputs. For each cell type that exhibited more than 3 synapses of input from or output onto mdIV terminals on both left and right sides of the body, we fully reconstructed and comprehensively reviewed a left and right pair of neurons. No unpaired medial neurons were found. For segmentally repeated cell types that exhibited multiple segments of connection, we chose to review examples from the segment with the most synapses from mdIVs, typically segment A1. Reconstructions here were performed by CMSM (30.2%, 104,335/345,917 nodes), IA (28.0%, 96,999/345,917 nodes), Javier Valdes Aleman (8.7%, 29,942/345,917 nodes), Laura Herren (8.1%, 28,165/345,917 nodes), Waleed Osman (7.1%, 24,727/345,917 nodes), and 3% or less each from several other contributors. Comprehensive reviews of arbors and synapses were performed by CMSM.

For annotation of the new L3v, we specifically targeted mdIV axons using characteristic anatomical features, particularly entry nerves and the ventromedial location of presynaptic boutons. Interneurons were identified based on cell body location, neuropil entry point of the primary neurite and characteristic branching structures. Partial neurons were reconstructed until good candidates were discovered. The reconstruction of 6 mdIV terminals and 12 specific LNs spanned 15.3 mm, 10035 synaptic inputs, and 13499 outputs. Reconstructions were performed by IA (50.8%, 91,836/180,753 nodes), SG (21.9%, 39,654/180,753 nodes), CMSM (19.3%, 34,927/180,753 nodes), AC (6.4%, 11,611/180,753 nodes), and Waleed Osman (1.5%, 2,725/180,753 nodes). Comprehensive reviews of arbors and synapses in the L3v were performed by SG and CMSM.

Analysis

Neurons were exported from CATMAID through custom python scripts and imported into python or MATLAB (The Mathworks, Inc.) environments for analysis. Analysis was performed with custom MATLAB scripts with statistics performed using Scipy and R. Neuronal morphology files and MATLAB code can be found at (*URL TO COME*).

References

[1] E Rebecka Björnfors and Abdeljabbar El Manira. Functional diversity of excitatory commissural interneurons in adult zebrafish. *eLife*, 5:10875, August 2016.

[2] Wesley B Grueber, Lily Y Jan, and Yuh Nung Jan. Different Levels of the Homeodomain Protein Cut Regulate Distinct Dendrite Branching Patterns of Drosophila Multidendritic Neurons. *Cell*, 112(6):805–818, March 2003.

[3] R K Murphey and A Chiba. Assembly of the cricket cercal sensory system: Genetic and epigenetic control. *Journal of neurobiology*, 21(1):120–137, January 1990.

[4] D Bucher. Animal-to-Animal Variability in Motor Pattern Production in Adults and during Growth. *The Journal of Neuroscience*, 25(7):1611–1619, February 2005.

[5] Haig Keshishian, Akira Chiba, Te Ning Chang, Marc S Halfon, Elizabeth W Harkins, Jill Jarecki, Lansheng Wang, Marydilys Anderson, Sydney Cash, Marnie E Halpern, and J rgen Johansen. Cellular mechanisms governing synaptic development inDrosophila melanogaster. *Journal of neurobiology*, 24(6):757–787, June 1993.

[6] Bo Guan, Beate Hartmann, Young-Ho Kho, Michael Gorczyca, and Vivian Budnik. The Drosophila tumor suppressor gene, dlg, is involved in structural plasticity at a glutamatergic synapse. *Current Biology*, 6(6):695–706, June 1996.

[7] Tobias M Rasse, Wernher Fouquet, Andreas Schmid, Robert J Kittel, Sara Mertel, Carola B Sigrist, Manuela Schmidt, Asja Guzman, Carlos Merino, Gang Qin, Christine Quentin, Frank F Madeo, Manfred Heckmann, and Stephan J Sigrist. Glutamate receptor dynamics organizing synapse formation in vivo. *Nature neuroscience*, 8(7):898–905, June 2005.

[8] G Kämper and R K Murphey. Maturation of an insect nervous system: Constancy in the face of change. *Comparative Biochemistry and Physiology Part A: Physiology*, 109(1):23–32, September 1994.

[9] Eve Marder and Jean-Marc Goaillard. Variability, compensation and homeostasis in neuron and network function. *Nature reviews Neuroscience*, 7(7):563–574, July 2006.

[10] Marco Tripodi, Jan Felix Evers, Alex Mauss, Michael Bate, and Matthias Landgraf. Structural Homeostasis: Compensatory Adjustments of Dendritic Arbor Geometry in Response to Variations of Synaptic Input. *PLoS Biology*, 6(10):e260, October 2008.

[11] Carlo NG Giachello and Richard A Baines. Regulation of motoneuron excitability and the setting of homeostatic limits. *Current opinion in neurobiology*, 43:1–6, April 2017.

[12] Adriane G Otopalik, Marie L Goeritz, Alexander C Sutton, Ted Brookings, Cosmo Guerini, and Eve Marder. Sloppy morphological tuning in identified neurons of the crustacean stomatogastric ganglion. *eLife*, 6:187, February 2017.

[13] Jean-Marc Goaillard, Adam L Taylor, David J Schulz, and Eve Marder. Functional consequences of animal-to-animal variation in circuit parameters. *Nature neuroscience*, 12(11):1424–1430, October 2009.

[14] B J Norris, A Wenning, T M Wright, and R L Calabrese. Constancy and Variability in the Output of a Central Pattern Generator. *The Journal of Neuroscience*, 31(12):4663–4674, March 2011.

[15] R C Roffman, B J Norris, and R L Calabrese. Animal-to-animal variability of connection strength in the leech heartbeat central pattern generator. *Journal of neurophysiology*, 107(6):1681–1693, March 2012.

[16] R Grashow, T Brookings, and E Marder. Compensation for Variable Intrinsic Neuronal Excitability by Circuit-Synaptic Interactions. *The Journal of Neuroscience*, 30(27):9145–9156, July 2010.

[17] Timothy O'Leary, Alex H Williams, Alessio Franci, and Eve Marder. Cell Types, Network Homeostasis, and Pathological Compensation from a Biologically Plausible Ion Channel Expression Model. *Neuron*, 82(4):809–821, May 2014.

[18] Astrid A Prinz, Dirk Bucher, and Eve Marder. Similar network activity from disparate circuit parameters. *Nature neuroscience*, 7(12):1345–1352, November 2004.

[19] Shin-Ya Takemura, C Shan Xu, Zhiyuan Lu, Patricia K Rivlin, Toufiq Parag, Donald J Olbris, Stephen Plaza, Ting Zhao, William T Katz, Lowell Umayam, Charlotte Weaver, Harald F Hess, Jane Anne Horne, Juan Nunez-Iglesias, Roxanne Aniceto, Lei-Ann Chang, Shirley Lauchie, Ashley Nasca, Omotara Ogundeyi, Christopher Sigmund, Satoko Takemura, Julie Tran, Carlie Langille, Kelsey Le Lacheur, Sari McLin, Aya Shinomiya, Dmitri B Chklovskii, Ian A Meinertzhagen, and Louis K Scheffer. Synaptic circuits and their variations within different columns in the visual system of Drosophila. *PNAS*, 112(44):13711–13716, November 2015.

[20] Tomoko Ohyama, Casey M Schneider-Mizell, Richard D Fetter, Javier Valdes Aleman, Romain Franconville, Marta Rivera-Alba, Brett D Mensh, Kristin M Branson, Julie H Simpson, James W Truman, Albert Cardona, and Marta Zlatic. A multilevel multimodal circuit enhances action selection in Drosophila. *Nature*, 520(7549):633–639, April 2015.

[21] Matthew E Berck, Avinash Khandelwal, Lindsey Claus, Luis Hernandez-Nunez, Guangwei Si, Christopher J Tabone, Feng Li, James W Truman, Rick D Fetter, Matthieu Louis, Aravinthan Dt Samuel, and Albert Cardona. The wiring diagram of a glomerular olfactory system. *eLife*, 5:450, May 2016.

[22] M F Zwart, O Randlett, J F Evers, and M Landgraf. Dendritic growth gated by a steroid hormone receptor underlies increases in activity in the developing Drosophila locomotor system. *PNAS*, 110(40):E3878–E3887, October 2013.

[23] James W Truman and Michael Bate. Spatial and temporal patterns of neurogenesis in the central nervous system of Drosophila melanogaster. *Developmental biology*, 125(1):145–157, January 1988.

[24] Richard Y Hwang, Lixian Zhong, Yifan Xu, Trevor Johnson, Feng Zhang, Karl Deisseroth, and W Daniel Tracey. Nociceptive Neurons Protect Drosophila Larvae from Parasitoid Wasps. *Current Biology*, 17(24):2105–2116, December 2007.

[25] Casey M Schneider-Mizell, Stephan Gerhard, Mark Longair, Tom Kazimiers, Feng Li, Maarten F Zwart, Andrew Champion, Frank M Midgley, Richard D Fetter, Stephan Saalfeld, and Albert Cardona. Quantitative neuroanatomy for connectomics in Drosophila. *eLife*, 5:1133, March 2016.

[26] David J Merritt, Andrew Hawken, and Paul M Whitington. The Role of the cut Gene in the Specification of Central Projections by Sensory Axons in Drosophila. *Neuron*, 10(4):741–752, April 1993.

[27] W B Grueber, B Ye, C H Yang, S Younger, K Borden, L Y Jan, and Y N Jan. Projections of Drosophila multidendritic neurons in the central nervous system: links with peripheral dendrite morphology. *Development*, 134(1):55–64, January 2007.

[28] Albert Cardona, Stephan Saalfeld, Stephan Preibisch, Benjamin Schmid, Anchi Cheng, Jim Pulokas, Pavel Tomancak, and Volker Hartenstein. An Integrated Micro- and Macroarchitectural Analysis of the Drosophila Brain by Computer-Assisted Serial Section Electron Microscopy. *PLoS Biology*, 8(10):e1000502, October 2010.

[29] W W Liu and R I Wilson. Glutamate is an inhibitory neurotransmitter in the Drosophila olfactory system. *PNAS*, 110(25):10294–10299, June 2013.

[30] Tihana Jovanic, Casey Martin Schneider-Mizell, Mei Shao, Jean-Baptiste Masson, Gennady Denisov, Richard Doty Fetter, Brett Daren Mensh, James William Truman, Albert Cardona, and Marta Zlatic. Competitive Disinhibition Mediates Behavioral Choice and Sequences in Drosophila. *Cell*, 167(3):858–870.e19, October 2016.

[31] John C Tuthill and Rachel I Wilson. Parallel Transformation of Tactile Signals in Central Circuits of Drosophila. *Cell*, 164(5):1046–1059, February 2016.

[32] Armen Stepanyants, Patrick R Hof, and Dmitri B Chklovskii. Geometry and Structural Plasticity of Synaptic Connectivity. *Neuron*, 34(2):275–288, April 2002.

[33] Florian Leiss, Ewa Koper, Irina Hein, Wernher Fouquet, Jana Lindner, Stephan Sigrist, and Gaia Tavosanis. Characterization of dendritic spines in the Drosophilacentral nervous system. *Developmental neurobiology*, 69(4):221–234, March 2009.

[34] T Binzegger. Axons in Cat Visual Cortex are Topologically Self-similar. *Cerebral Cortex*, 15(2):152–165, July 2004.

[35] Maarten F Zwart, Stefan R Pulver, James W Truman, Akira Fushiki, Richard D Fetter, Albert Cardona, and Matthias Landgraf. Selective Inhibition Mediates the Sequential Recruitment of Motor Pools. *Neuron*, 91(3):615–628, August 2016.

[36] Akira Fushiki, Maarten F Zwart, Hiroshi Kohsaka, Richard D Fetter, Albert Cardona, and Akinao Nose. A circuit mechanism for the propagation of waves of muscle contraction in Drosophila. *eLife*, 5:612, February 2016.

[37] Ellie S Heckscher, Aref Arzan Zarin, Serge Faumont, Matthew Q Clark, Laurina Manning, Akira Fushiki, Casey M Schneider-Mizell, Richard D Fetter, James W Truman, Maarten F Zwart, Matthias Landgraf, Albert Cardona, Shawn R Lockery, and Chris Q Doe. Even-Skipped+ Interneurons Are Core Components of a Sensorimotor Circuit that Maintains Left-Right Symmetric Muscle Contraction Amplitude. *Neuron*, 88(2):314–329, October 2015.

[38] William F Tobin, Rachel I Wilson, and Wei-Chung Allen Lee. Wiring variations that enable and constrain neural computation in a sensory microcircuit. *eLife*, 6:894, May 2017.

[39] Stefanie Ryglewski, Fernando Vonhoff, Kathryn Scheckel, and Carsten Duch. Intra-neuronal Competition for Synaptic Partners Conserves the Amount of Dendritic Building Material. *Neuron*, 93(3):632–645.e6, February 2017.

[40] B D Pfeiffer, A Jenett, A S Hammonds, T T B Ngo, S Misra, C Murphy, A Scully, J W Carlson, K H Wan, T R Laverty, C Mungall, R Svirskas, J T Kadonaga, C Q Doe, M B Eisen, S E Celniker, and G M Rubin. Tools for neuroanatomy and neurogenetics in Drosophila. *PNAS*, 105(28):9715–9720, July 2008.

[41] B D Pfeiffer, T T B Ngo, K L Hibbard, C Murphy, A Jenett, J W Truman, and G M Rubin. Refinement of Tools for Targeted Gene Expression in Drosophila. *Genetics*, 186(2):735–755, October 2010.

[42] Sato, T. A Modified Method for Lead Staining of Thin Sections. *Journal of Electron Microscopy*, 1968.

[43] Christian Suloway, James Pulokas, Denis Fellmann, Anchi Cheng, Francisco Guerra, Joel Quispe, Scott Stagg, Clinton S Potter, and Bridget Carragher. Automated molecular microscopy: The new Leginon system. *Journal of Structural Biology*, 151(1):41–60, July 2005.

[44] S Saalfeld, A Cardona, V Hartenstein, and P Tomancak. As-rigid-as-possible mosaicking and serial section registration of large ssTEM datasets. *Bioinformatics*, 26(12):i57–i63, June 2010.

[45] Albert Cardona, Stephan Saalfeld, Johannes Schindelin, Ignacio Arganda-Carreras, Stephan Preibisch, Mark Longair, Pavel Tomancak, Volker Hartenstein, and Rodney J Douglas. TrakEM2 Software for Neural Circuit Reconstruction. *PloS one*, 7(6):e38011, June 2012.

[46] Stephan Saalfeld, Richard Fetter, Albert Cardona, and Pavel Tomancak. Elastic volume reconstruction from series of ultra-thin microscopy sections. *Nature methods*, 9(7):717–720, June 2012.

[47] S Saalfeld, A Cardona, V Hartenstein, and P Tomancak. CATMAID: collaborative annotation toolkit for massive amounts of image data. *Bioinformatics*, 25(15):1984–1986, July 2009.

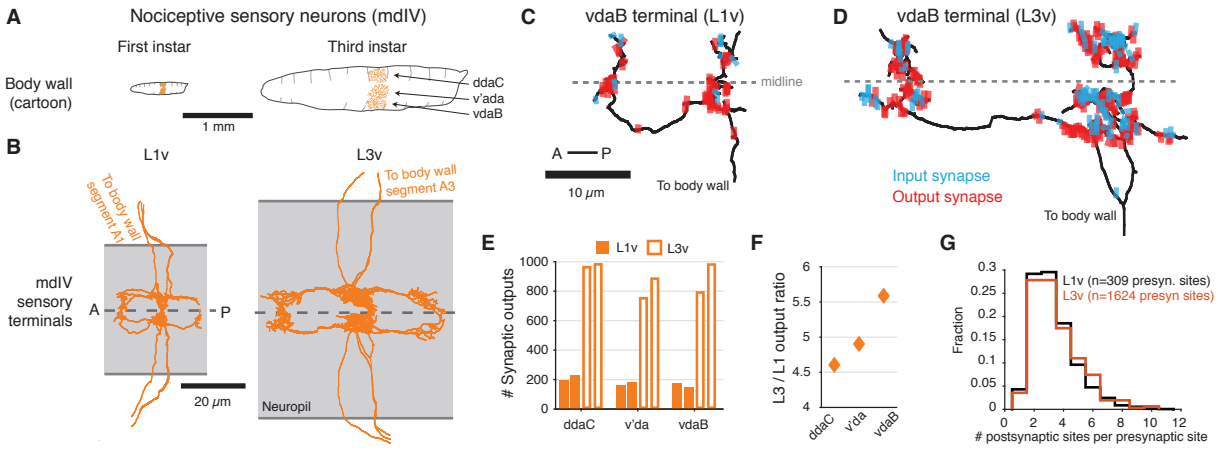

Figure 1: **Structure of mdIV terminals through postembryonic development. A**, The dendritic fields of the 3 mdIV sensory neurons (orange, cartoon) from a single hemisegment at early and late larval development, saggital view, same scale. Dorsal, lateral, and ventral mdIV types indicated. **B**, Dorsal view of all mdIV terminals from a single abdominal segment in the L1v (segment A1, 1st instar larva) and L3v (segment A3, 3rd instar larva), same scale, reconstructed from EM. The vertical extent of the gray box indicates the width of the neuropil. Anterior is to left, dashed line indicates midline. **C,D**, Dorsal view of an example vdaB terminal with synapses from the L1v (**C**) and the L3v (**D**), same scale. Red lines indicate output synapses, cyan lines input synapses; Dashed line indicates midline. **E**, Number of synaptic outputs made by each mdIV terminal. L1v (solid bars), L3v (empty bars); left/right bar corresponds to left/right neuron. **F**, Fold-change in synaptic outputs in the L1v and L3v. For each mdIV subtype, left and right terminals were averaged. **G**, Normalized histogram of number of synaptic contacts per presynaptic site on mdIV terminals (No significant difference, p = 0.5641, two-sided Kolmogorov-Smirnov test).

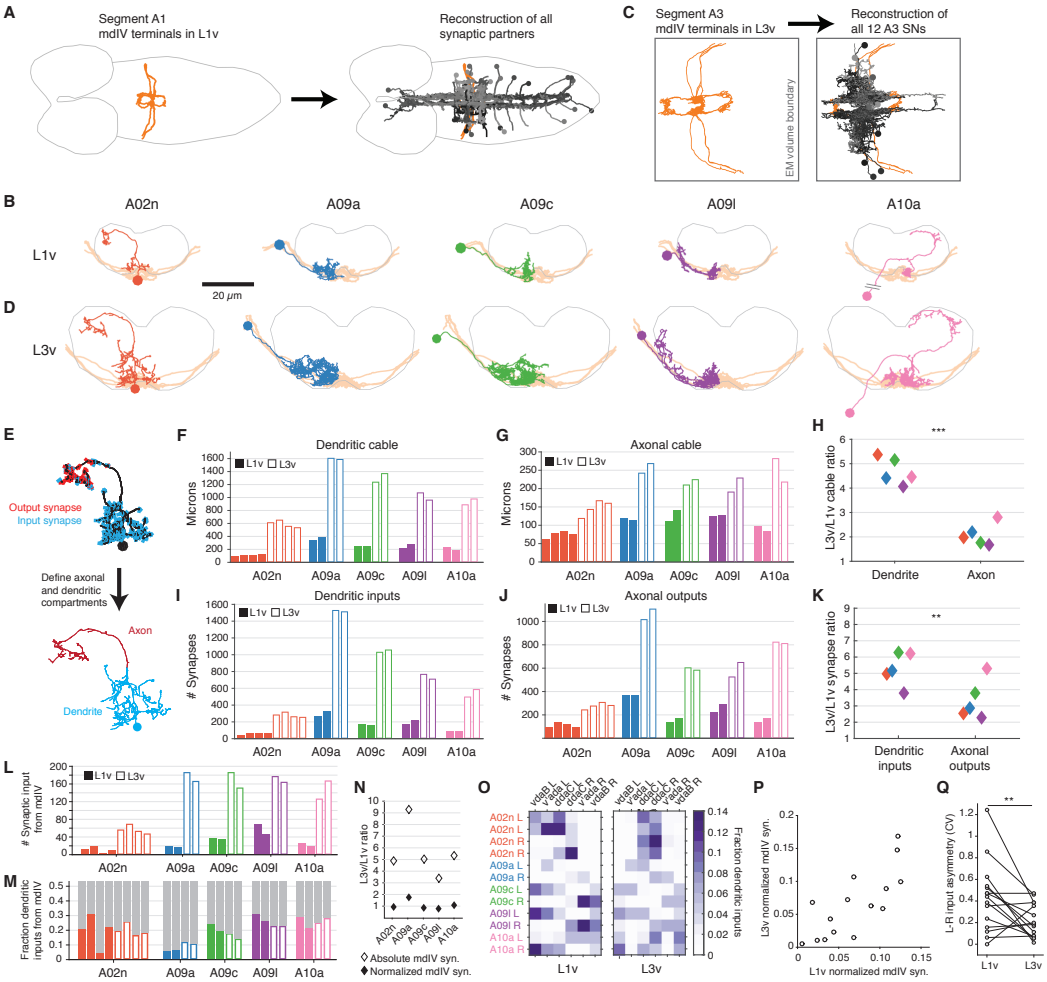

Figure 2: **Postembryonic development of morphology and connectivity of LNs connected to mdIVs**. **A**, All synaptic partners (dark colors) of the mdIVs (orange) in segment A1 were reconstructed in the L1v (See Supplemental Atlas for all neurons). Dorsal views, grey outline indicates CNS boundary. Anterior to left. **B** Posterior views of an example of each LN cell type in the L1v. See main text and Figure 2—figure supplement 1 for definition of LNs. Faded orange shows mdIV terminals, grey outline shows neuropile extent. Dorsal is up. **C**, The 12 LNs (dark colors) whose complete dendritic extent would be contained within the EM volume were reconstructed in the L3v (grey box indicates volume limits). Anterior to left. **D**, Posterior views of an example of each type of LN in the L3v volume. Images and scale as in **B**. **E**, All neurons were split into axonal and dendritic compartments based on separable input and output domains (A02n shown). **F**, Total dendritic cable length for all LNs. **G**, Total axonal cable length for all LNs. **H**, Fold-change in cable between the L1v and L3v for LN dendrites and axons, separately. Dendrites increase significantly more than axons (two-sided t-test). **I**, Number of inputs onto LN dendrites. **J**, Number of outputs from LN axons. **K**, Fold-increase of LN dendritic inputs and axonal outputs. Dendritic inputs increase significantly more (two-sided t-test). **L**, Number of synaptic inputs onto LNs from mdIV terminals in the same segment. **M**, Inputs from mdIV terminals normalized by the total number of dendritic inputs for each LN. **N**, Fold-increase in absolute and normalized synaptic inputs for each LN. **O**, Heatmap showing normalized input from each mdIV onto each LN. **P**, Normalized input from mdIVs onto LNs is strongly correlated across animals and developmental time points. (Pearson's r = 0.77, $p<0.001$ to be different from zero). **Q**, Coefficient of variation for mdIV-to-LN connection strength (in synapse count) in the L1v and L3v. Variability decreases significantly (two-sided paired t-test). n.s. not significant; *: $p<0.05$. **: $p<0.01$. ***: $p<0.001$.

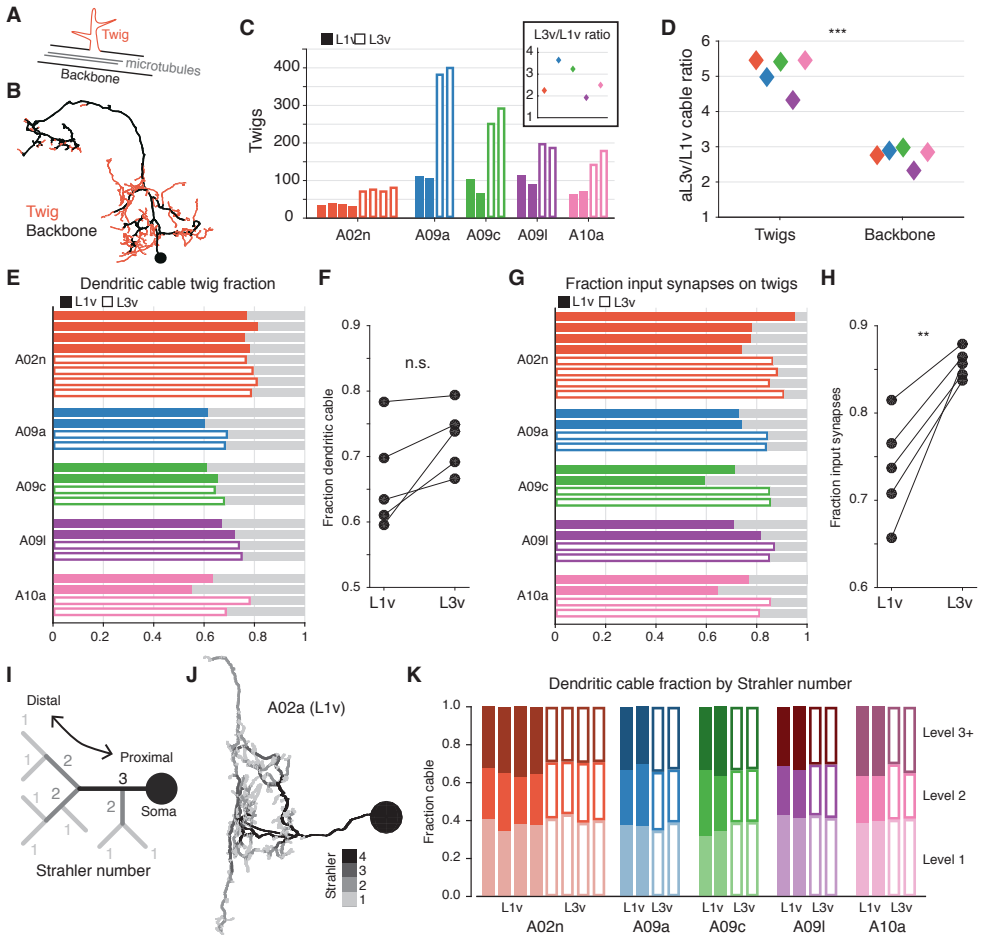

Figure 3: **Twig and backbone compartments through postembryonic development**. **A**, Definition of microtubule-containing "backbone" (black) and microtubule-free, spine-like "twigs" (red). **B**, Example A02n cell (L3v) where all twigs are labeled, posterior view. **C**, Number of twigs in each LN in the L1v and L3v. Inset: Fold-change in number of twigs between the L1v and L3v. **D**, Fold-change in amount of cable comprised of twigs or backbone in the L1v and L3v. Twigs increase significantly more than backbone (two sided t-test). **E**, Fraction of dendritic cable comprised of twigs for all LNs. **F**, The average fraction of dendritic cable comprised of twigs per cell type was not significantly different across development (two sided, paired t-test). **G**, Input synapses that contact twigs as a fraction of all input synapses for all LNs. **H**, The fraction of input synapses that are onto twigs increased significantly (two-sided, paired t-test). **I**, Cartoon definition of Strahler number. Terminal tips are defined to have Strahler number one. Where two branches with the same Strahler number converge, Strahler number increments by one. The most core, proximal neurites thus have the highest Strahler number. **J**, An example A09a cell with branches labeled by Strahler number (Dorsal view). **K**, Fraction of dendritic cable for each LN by Strahler number. The relative amount of cable with low Strahler number (*i.e.* distal) is strongly conserved between the L1v and L3v neurons. n.s. not significant; *: $p<0.05$. **: $p<0.01$. ***: $p<0.001$.

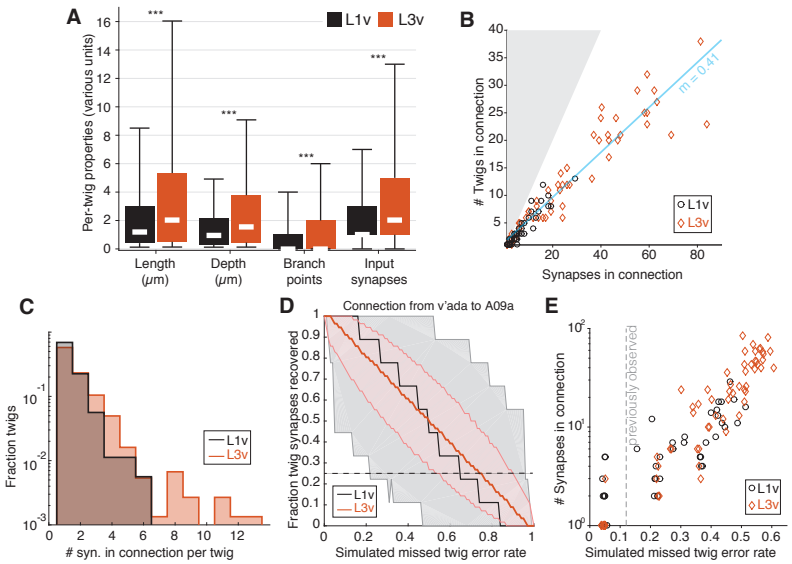

Figure 4: **Twig properties across postembryonic development**. **A**, Distribution of morphological and synaptic properties of distinct twigs in the L1v and L3v LNs. Total twig length and maximum twig depth are in μm, branch points and synapses are integer. Boxes are interquartile intervals, white dashes are median values, and whiskers correspond to 5/95 percentiles. Wilcoxon rank sum test with Bonferroni correction. **B**, Number of distinct twigs in a connection versus number of synapses in the same connection. The blue line indicates a linear fit to connections with five or more synapses (slope shown). The grey box corresponds to the disallowed situation of more twigs connected than synapses. **C**, Histogram of number of synapses per twig in each mdIV-to-LN connection. **D**, The fraction of synapses in the connection from a v'ada to an A09a in the L1v (9 synapses onto twigs) and L3v (56 synapses onto twigs) recovered after simulated random omission of twigs, as a function of omission probability (N=5000 simulations). Thick lines show median value, shaded region the 5/95 percentile value. The dashed horizontal line indicates the 25% of synapses recovered. **F**, Maximum error rate permitting the recovery of 25% of synapses with probability>0.05 for each observed mdIV-to-LN connection (i.e. where the horizontal dashed line crosses into the shaded area in **E**). Each data point is a single mdIV axon's synapses with a single LN. The vertical line indicates the error rate for twigs found previously for manual annotation of motor neurons [25]. n.s. not significant; *: $p<0.05$. **: $p<0.01$. ***: $p<0.001$.